The Astrophysical Journal Supplement Series, 154:322–327, 2004 September

RCW 49 AT MID-INFRARED WAVELENGTHS: A GLIMPSE FROM THE *SPITZER SPACE TELESCOPE*

E. Churchwell,[1] B. A. Whitney,[2] B. L. Babler,[1] R. Indebetouw,[1] M. R. Meade,[1] Christer Watson,[1] M. J. Wolff,[2] M. G. Wolfire,[3] T. M. Bania,[4] R. A. Benjamin,[5] D. P. Clemens,[4] Martin Cohen,[6] K. E. Devine,[1] J. M. Dickey,[7] F. Heitsch,[8] J. M. Jackson,[4] H. A. Kobulnicky,[9] A. P. Marston,[10] J. S. Mathis,[1] E. P. Mercer,[4] J. R. Stauffer,[11] and S. R. Stolovy[11]

Received 2004 March 23; accepted 2004 May 7

ABSTRACT

The luminous, massive star formation region RCW 49, located in the southern Galactic plane, was imaged with the Infrared Array Camera (IRAC) on the *Spitzer Space Telescope* as part of the Galactic Legacy Infrared Mid-Plane Survey Extraordinaire (GLIMPSE) program. The IRAC bands contain polycyclic aromatic hydrocarbon (PAH) features at 3.3, 6.2, 7.7, and 8.6 μm, as well as the Brα line. These features are the major contributors to the diffuse emission from RCW 49 in the IRAC bands. The *Spitzer* IRAC images show that the dust in RCW 49 is distributed in a network of fine filaments, pillars, knots, sharply defined boundaries, bubbles, and bow shocks. The regions immediately surrounding the ionizing star cluster and W-R stars are evacuated of dust by stellar winds and radiation. The IRAC images of RCW 49 suggest that the dust in RCW 49 has been sculpted by the winds and radiation from the embedded luminous stars in the inner 5′ (inner ~6 pc) of the nebula. At projected angular radii $\phi > 5'$ from the central ionizing cluster, the azimuthally averaged infrared intensity falls off as $\sim\phi^{-3}$. Both high-resolution radio and mid-IR images suggest that the nebula is density bounded along its western boundary. The filamentary structure of the dust in RCW 49 suggests that the nebula has a small dust filling factor and, as a consequence, the entire nebula may be slightly density bounded to H-ionizing photons.

Subject headings: astrochemistry — dust, extinction — H II regions — infrared: ISM — ISM: lines and bands

1. INTRODUCTION

Luminous H II regions (i.e., massive star formation regions) play a major role in galaxies by illuminating and ionizing the ambient interstellar medium (ISM), driving turbulence and sculpting the structure of gas and dust via stellar winds and supernova explosions, and enriching the ISM via supernova explosions and processed stellar wind particles. Massive star formation is a key to galaxy morphology and the structure and energetics of the ISM in galaxies. NGC 3247, usually referred to as RCW 49 (Rogers et al. 1960), is a large, optically visible, and luminous H II region located in the southern Galactic plane at $l = 284.^{\circ}3$, $b = -0.^{\circ}3$. The H II region is ionized by the compact cluster Westerlund 2 (hereafter W2), which contains at least a dozen OB stars, five of which are O7 V stars, one of which is an O6 V, and two of which are W-R stars (Moffat & Vogt 1975; Moffat et al. 1991, hereafter MSP91; Carraro & Munari 2004). The two W-R–type stars are WR 20a (WN 7) and WR 20b (WN 6:h; van der Hucht 2001).

RCW 49 has been detected at X-rays from 0.2 to 4.5 keV by Hertz (1983), Hertz & Grindlay (1984), and Goldwurm et al. (1987) and from 0.1 to 2.4 keV by Belloni & Mereghetti (1994). Both X-ray point sources and extended emission have been reported. RCW 49 has also been observed in molecular and atomic line surveys of OH (Caswell 1997, 1998), CH_3OH (Caswell 1997), H_2O (Batchelor et al. 1980), H_2CO (Caswell & Haynes 1987; Whiteoak & Gardner 1974), and H109α and/or H110α lines (Wilson et al. 1970; Caswell & Haynes 1987). It has also been imaged in the radio continuum by Goss & Shaver (1970), Shaver & Goss (1970), Haynes et al. (1978, 1979), and Whiteoak & Uchida (1997, hereafter WU97).

The distance to RCW 49 is uncertain. MSP91 report a luminosity distance to the cluster of 7.9 kpc; however, other investigators have reported distances of 2.3 (Manchester et al. 1970; Brand & Blitz 1993; WU97) and 5.0 kpc (Westerlund 1960; Manchester et al. 1969; Caswell & Haynes 1987). The radio recombination lines toward RCW 49 have a radial velocity of ~0 km s^{-1} (Wilson et al. 1970; Caswell & Haynes 1987), indicating a kinematic distance of about 4.2 kpc, but peculiar motions of $\pm$10 km s^{-1} would place the nebula anywhere from ~2.2 to ~5.8 kpc. Carraro & Munari (2004) report a photometric distance of 6.4 $\pm$ 0.4 kpc, similar to the 5.75 kpc quoted by van der Hucht (2001) for WR 20a. We adopt the far kinematic distance of 4.2 kpc based on the H I 21 cm absorption line profile (Goss et al. 1972; McClure-Griffiths et al. 2001) toward RCW 49, which shows deep absorption out to the tangent point velocity of -29 km s^{-1}. Until the discrepancy between the photometric and kinematic distances is resolved, the distance must be considered to be uncertain by roughly $\pm$2 kpc. At a distance of 4.2 kpc, 1″ corresponds to 0.020 pc.

[1] Department of Astronomy, University of Wisconsin, 475 North Charter Street, Madison, WI 53706.
[2] Space Science Institute, 4750 Walnut Street, Suite 205, Boulder, CO 80301.
[3] Department of Astronomy, University of Maryland, College Park, MD 20742-2421.
[4] Institute for Astrophysical Research, Boston University, 725 Commonwealth Avenue, Boston, MA 02215.
[5] Department of Physics, University of Wisconsin, 800 West Main Street, Whitewater, WI 53190.
[6] Radio Astronomy Laboratory, University of California, 601 Campbell Hall, Berkeley, CA 94720.
[7] Department of Astronomy, University of Minnesota, 116 Church Street SE, Minneapolis, MN 55455.
[8] Institute for Astronomy, University of Munich, Scheinerstrasse 1, 81679 Munich, Germany.
[9] Department of Physics and Astronomy, University of Wyoming, P.O. Box 3905, Laramie, WY 82072.
[10] European Space Research and Technology Center, Space Science Astrophysics Department, European Space Agency, Keplerlaan 1 Postbus 299, AG NL-2200 Noordwijk, Netherlands.
[11] *Spitzer* Science Center, California Institute of Technology, MC 314-6, 1200 East California Boulevard, Pasadena, CA 91125.

A key issue that we address in this paper is the morphology of dust associated with RCW 49. An associated issue is the ionization source of the warm ionized medium (WIM), the layer of diffuse ionized hydrogen above and below the Galactic plane, often referred to as the Reynolds layer.

2. OBSERVATIONS AND DATA REDUCTION

The data reported here were obtained on 2003 December 23, with the Infrared Array Camera (IRAC; Fazio et al. 2004) on the *Spitzer Space Telescope*. IRAC has four wavelength bands centered at 3.6, 4.5, 5.8, and 8.0 μm (hereafter [3.6], [4.5], [5.8], and [8.0], respectively), each of which has a field of view (FOV) of $\sim 5\farcm2 \times 5\farcm2$. All four bands are observed simultaneously. The [3.6] and [5.8] FOVs are coincident on the sky and the [4.5] and [8.0] FOVs are coincident, but the center positions of the two pairs are offset by $6\farcm73$. The pixel size in all four bands is $\sim 1\farcs22$. The FWHM of the point-spread functions was $1\farcs63$, $1\farcs70$, $1\farcs85$, and $1\farcs94$ at [3.6], [4.5], [5.8], and [8.0], respectively. More information on IRAC is available from Fazio et al. (2004) and from the *Spitzer* Science Center Observer Support Web site.[12]

The Galactic Legacy Infrared Mid-Plane Survey Extraordinaire (GLIMPSE) is a fully sampled survey of the inner two-thirds of the Galactic plane ($l = \pm 10^\circ - 65^\circ$, $b = \pm 1^\circ$; total area ~ 220 deg^2) in all four IRAC bands. This program is described in detail by Benjamin et al. (2003). The GLIMPSE program was validated using early observations taken using precisely the same observing strategy that will be used by GLIMPSE. We refer to these data as the observing strategy validation (OSV) data. The OSV[13] covered an area of about $1\fdg7 \times 0\fdg7$ centered on RCW 49. The area was imaged using half-frame steps in one telescope coordinate and slightly less than a frame offset in the perpendicular direction. Every point in the OSV area was observed a minimum of 10 times. A total of 1648 frames per IRAC band, each exposed for 1.2 s, were mosaicked to form the final images. The minimum total exposure time per pixel was 12 s, and the total observing time was 10 hr.

The calibrated data from the *Spitzer* Science Center (SSC pipeline ver. S9.01) were processed through the GLIMPSE pipeline reduction system (Benjamin et al. 2003; Whitney et al. 2004). Point sources were extracted from each frame using a modified version of DAOPHOT (Stetson 1987), and the individual frames at a given band were mosaicked using MONTAGE[14] to produce an image of the entire field at each band.

3. *SPITZER* MID-INFRARED IMAGES OF RCW 49

In the top panel of Figure 1 (Plate 1) we show a three-color ([3.6], [5.8], and [8.0]) image of RCW 49 with various nebular and stellar features indicated. In the bottom panel of Figure 1 we show a three-color (J, H, K) Two Micron All Sky Survey[15] (2MASS) image of RCW 49 for comparison. There is a striking difference between the faint, diffuse emission at J, H, and K bands and the bright, diffuse, highly structured emission in the IRAC bands. At J, H, and K, the diffuse emission is primarily a combination of scattered light from the W2 cluster and Brγ line emission. Only faint traces of the diffuse emission seen in the IRAC bands are apparent at J, H, and K bands. In the IRAC bands, the diffuse emission is produced primarily by polycyclic aromatic hydrocarbon (PAH) features and Brα line emission, which we discuss below.

In Figure 2 (Plate 2) we show two sets of three-color images centered on RCW 49 composed of subsets of the OSV data ($\sim$360 frames per band). The top panels show the entire nebula; the bottom panels are zoomed in by a factor of 2 centered on the W2 cluster. We assign blue to the shortest wavelength band, green to the intermediate band, and red to the longest wavelength band. The left panels are composites of the [3.6], [4.5], and [5.8] bands, and the right panels are composites of the [3.6], [5.8], and [8.0] bands. These color combinations were chosen to highlight particular properties of the images described below. The same general features are seen in both of the three-color images, but there are important differences in the details that we discuss below. IRAC [3.6], [5.8], and [8.0] bands each contain PAH emission features: 3.3 μm in the [3.6] band, 6.2 μm in the [5.8] band, and 7.7 and 8.6 μm in the [8.0] band (Draine 2003). These features are excited by UV radiation and as a consequence become bright in the neighborhood of a hot star if it is embedded in or surrounded by dust. Small dust grains can also be stochastically heated by absorption of UV radiation and reradiate at mid-IR wavelengths.

IRAC [4.5] contains the bright hydrogen recombination line Brα (4.05 μm). The integrated radio continuum emission from RCW 49 was used to predict a Brα flux within $\sim$20% of the nonstellar flux observed in the [4.5] band integrated over RCW 49. We conclude that Brα dominates the extended emission in IRAC [4.5] toward bright H II regions.

Colors intermediate between red and green in Figures 1 and 2 indicate a combination of Brα line emission ([4.5] band) and PAH emission ([3.6], [5.8], and [8.0] bands) throughout RCW 49. The reddish shades in Figure 2 indicate the distribution of warm dust emitting primarily in the 6.2 μm PAH feature in the [5.8] band (all panels of Fig. 2) and the 7.7 and 8.6 μm PAH features in the [8.0] band (right panels of Fig. 2). Main-sequence stars with photospheres hotter than $\sim$1000 K appear blue in IRAC colors, except for the most reddened ones, and are brightest at [3.6] and [4.5]. All IRAC images of RCW 49 show basically the same features and extents, but their brightnesses are quite different. The diffuse emission systematically and sharply increases from [3.6] to [8.0] (see Fig. 3). In addition, the [4.5] band (dominated by Brα) shows the same general features seen in the other bands (dominated by PAH features), although they seem to be less sharply defined in [4.5].

The dust features that produce the bright, diffuse emission associated with RCW 49 show a number of interesting properties. The major features are illustrated in Figure 3, which shows profiles at each IRAC band of the azimuthally averaged intensity as a function of projected angle ϕ from W2. Among these is the core of the W2 cluster inside a radius of $\phi \sim 10''$, a dust-evacuated region out to $\phi \sim 60''$, a bright shell of swept-up dust and gas at $\phi \sim 100''$, and a region of constant or slightly decreasing intensity between $\phi \sim 150''$ and $\sim 300''$. We refer to the radius at $\phi \sim 300''$ as the "transition boundary," beyond which the mean intensity decreases with projected radius as

[12] Available at http://ssc.spitzer.caltech.edu/ost.

[13] All 20 Astronomical Observation Requests (AORs) of the OSV data have program identification number (PID) 195.

[14] See http://montage.ipac.caltech.edu. MONTAGE was funded by the National Aeronautics and Space Administration's Earth Science Technology Office, Computational Technnologies Project, under Cooperative Agreement NCC5-626 between NASA and the California Institute of Technology.

[15] The Two Micron All Sky Survey is a joint project of the University of Massachusetts and the Infrared Processing and Analysis Center/California Institute of Technology, funded by the National Aeronautics and Space Administration and the National Science Foundation.

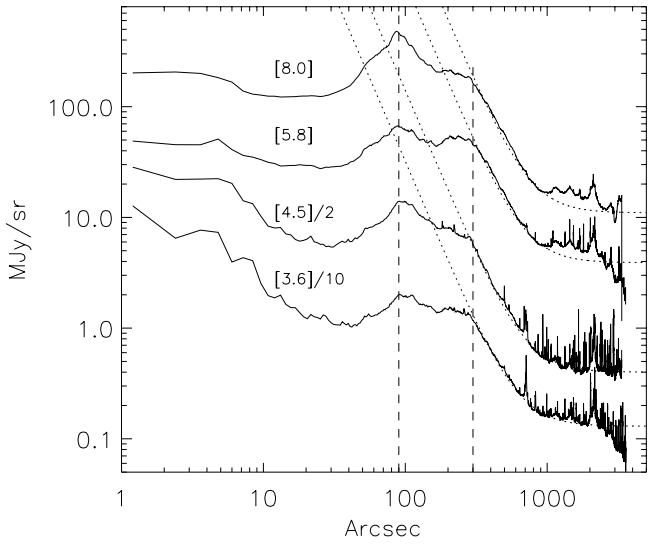

FIG. 3.—Projected azimuthally averaged radial profiles of the emission from RCW 49 centered on the W2 cluster. The dotted curves are power laws of slope −3. The two vertical dashed lines indicate the inner swept-up shell at angular radius $\phi \sim 100''$ and $300''$; the second one indicates the transition boundary beyond which the mean brightness decreases as $\sim\phi^{-3}$. The central wavelengths of the IRAC bands, in μm, are indicated in square brackets. The intensity of the [3.6] band is divided by 10 and [4.5] is divided by 2. The ϕ^{-3} dependence flattens at $\sim 1000''$ because the intensity merges with the background.

$\sim\phi^{-3}$. The region between $150''$ and $300''$ we refer to as the plateau. These features are illustrated in Figure 3 and are apparent in Figures 1 and 2. The ϕ^{-3} dependence of the azimuthally averaged intensity on *projected* distance from the W2 cluster is consistent with optically thin emission reradiated by dust with emissivity $\epsilon_d \propto n_d/r^2$, where n_d is the space density of dust, r is the three-dimensional distance from the center of W2, and r^{-2} accounts for the geometrical dilution of the radiation field from the W2 cluster. We assume that $n_d \propto r^{-2}$, so that $\epsilon_d \propto r^{-4}$ resulting in a ϕ^{-3} dependence of the azimuthally averaged intensity, as observed.

The angular diameter (to the background level) of the dust emission from RCW 49 in the IRAC bands is $\sim 33' \times 18'$ ($\sim 40 \times 22$ pc for a distance of 4.2 kpc). The major axis has a position angle of $\sim 340^\circ$ ($\sim 20^\circ$ west of north). By comparison, the Molonglo Observatory Synthesis Telescope (MOST) 843 MHz image of WU97 has a bright emission core of diameter $12'$, but emission filaments are detected as far as $30'$ to the west and 1° to the northeast of W2. Thus, the total extent of the IRAC images is somewhat larger than the radio core diameter but smaller than the extent of some of the radio filaments. Clearly, some H-ionizing photons extend well beyond the near- to mid-IR images of RCW 49 in the directions where the radio filaments are observed (west and northeast). The radio and mid-IR images show that dust either coexists with ionized gas or is embedded in neutral gas clumps intimately mixed with ionized gas (i.e., as a matrix of radio continuum from interclump regions and PAH from clumps) in RCW 49.

The transition boundary is apparent in Figures 1 and 2 as a ring of eroded dust pillars that point toward the W2 cluster. The pillars appear to have been sculpted by the winds and radiation from the massive stars in the cluster and may represent remnants of Rayleigh-Taylor instabilities or dense cloud cores possibly containing embedded low-mass protostars like those in M16 (Hester et al. 1996; Scowen et al. 1998). The intensity interior to $\phi \sim 300''$ does not follow any simple analytic function with radius as it does outside this region. The average intensities systematically increase from [3.6] to [8.0] (see Fig. 3). The integrated flux densities of *diffuse* emission (i.e., measured on images in which point sources have been extracted) in the [3.6]–[8.0] bands are 233, 221, 860, and 3246 Jy, respectively, which quantitatively shows the large increase in diffuse emission in the [5.8] and [8.0] bands relative to the [3.6] and [4.5] bands. The diffuse flux densities in bands [5.8] and [8.0] have been reduced by factors of $\sim$0.63 and $\sim$0.69, respectively, as per SSC calibration recommendations.

The brightest emission, at both radio continuum and mid-IR wavelengths, lies between the core of the W2 cluster and WR 20b. WU97 postulated that this region has been compressed by shocks from both sides by winds from the W2 cluster and WR 20b. In this region, a pattern of narrow, bright, wavy filaments is apparent (see Fig. 1); the filaments are most clearly defined in IRAC [5.8]. A medium that is shocked and compressed from two sides (see Vishniac 1994; Blondin & Marks 1996; Garcia-Segura & Franco 1996) will produce wavy structures known as "Vishniac instabilities."

One of the most striking aspects of the images shown in Figure 2 is the complex, filamentary structure of the dust distribution in RCW 49. The index of the spatial separation spectrum, n [$P(k) \propto k^{-n}$, where $P(k)$ is the Fourier transform of the two-point correlation function of intensities at separation $1/k$], varies between 1.8 and 1.4 for spatial scales ranging from $1''.2$ to $40''$ within boxes $40''$ on a side distributed over the face of the nebula. The mean value of n is consistent with a spectral index of 1.67, the value associated with turbulence in the diffuse ISM. The striking feature about the size scales of dust structures in RCW 49 is their presence down to our resolution limit ($\sim$0.03 pc), although most of the power is in larger scale structures.

The IRAC images of RCW 49 suggest that little of the volume is occupied by dusty material. Most of the diffuse features seen in the [5.8] band (mostly a dust tracer) are also seen in the [4.5] band (mostly an H^+ tracer via Brα emission). The feature boundaries do not seem quite as sharply defined at [4.5] as they are at [5.8], although this is difficult to quantify because of the large difference in brightness at the two bands.

The network of thin filaments, pillars, and sharp boundaries hints that the nebula may be slightly density bounded. H-ionizing radiation propagates $\geq 30'$ west of W2 (the direction in which radio ring A is disrupted) and at least 1° to the northeast of W2 as shown by radio continuum filaments. To establish quantitatively the rate at which UV radiation escapes is impossible without more and deeper photometry of the stellar content of the W2 cluster. The UV photon luminosity required to ionize the nebula is $\sim 5.7 \times 10^{50} [D(\mathrm{kpc})/4.2\ \mathrm{kpc}]^2$ s^{-1}, based on the 5 GHz flux density of Goss & Shaver (1970). The five O7 V, one O6 V, and two W-R stars listed by MSP91, Moffat & Vogt (1975), and Carraro & Munari (2004) can provide most of the UV flux required for ionization, assuming the stellar photon fluxes of Vacca et al. (1996) and a distance of 4.2 kpc. There may, of course, be additional B stars and possible O stars that are hidden at visible wavelengths by extinction; the average extinction is $A_V \sim 5$ mag (Carraro & Munari 2004), but the youngest stars could have much larger local extinctions. Whitney et al. (2004) have found $\sim$300 highly reddened protostar candidates in RCW 49, indicating that star formation is an ongoing process in RCW 49. Until all the optically obscured stars are identified and their spectral types determined, we cannot establish the fraction of ionizing flux that escapes the nebula. Because the radial velocity of

RCW 49 is $\sim$0 km s^{-1}, Hα, H I 21 cm, and CO gas lying above or below (in latitude) RCW 49 is confused with local ionized and neutral gas. Consequently, we have been unable to determine the ionization state of gas located above or below RCW 49, which might give some indication of leakage of UV from the nebula. Improving this estimate is important because ionization of the Reynolds layer (the diffuse ionized layer of hydrogen above and below the Galactic plane; Reynolds et al. 1973) could be accounted for if only $\sim$15% of the UV photons from OB stars in the disk of the Galaxy escape into the lower halo (Reynolds 1984). This is a small fraction, and to determine if density boundedness at this level occurs will require an accurate census of hot stars in the cluster, stellar atmosphere model UV fluxes accurate to less than 15% error and an accurate determination of the fraction of ionizing UV absorbed by dust in the nebula. GLIMPSE will identify any optically obscured candidate OB stars from which a better estimate of the total stellar UV photon flux can be determined.

4. SUMMARY AND CONCLUSIONS

The *Spitzer* IRAC observations of RCW 49 (NGC 3247) have revealed the following:

1. Dust coexists with ionized gas in RCW 49 or else is embedded in neutral gas intimately mixed with ionized gas.
2. At radii less than $\sim5'$ from the W2 cluster, the dust has been sculpted by stellar winds and radiation.
3. At radii greater than $\sim5'$ from the W2 cluster, the mean intensity at [3.6]–[8.0] decreases with projected angle as ϕ^{-3}, consistent with optically thin emission, dust emissivity proportional to the space density of dust, dust density decreasing with true distance from the W2 cluster as r^{-2}, and the radiation field decreasing as r^{-2} as expected for geometrical dilution.
4. Dust is distributed in a complex network of thin filaments, pillars, sharp boundaries, and knots, suggesting that the dust filling factor is small. The size scales of dust structures have a spectrum index similar to that of turbulence in the ISM with structure present down to our resolution limit ($\sim$0.03 pc).

The observations described here and by Whitney et al. (2004) and Mercer et al. (2004) demonstrate that the GLIMPSE program has great potential to reveal the distributions of dust and stars in the inner Galaxy from which the number and locations of spiral arms, the Galactic stellar scale length, and properties of massive star formation can be determined. GLIMPSE also has a high probability for serendipitous discoveries.

We acknowledge the invaluable assistance of Stephan Jansen in maintaining the computational resources of the GLIMPSE computing network. We also thank the referee, Miller Goss, who made several suggestions that improved the content and presentation of this paper. Support for this work, part of the *Spitzer* Space Telescope Legacy Science Program, was provided by NASA through contracts 1224653 (Univ. Wisconsin Madison), 1225025 (Boston Univ.), 1224681 (Univ. Maryland), 1224988 (Space Science Institute), 1242593 (Univ. California Berkeley), 1253153 (Univ. Minnesota), 11253604 (Univ. Wyoming), and 1256801 (Univ. Wisconsin Whitewater) by the Jet Propulsion Laboratory, California Institute of Technology under NASA contract 1407.

REFERENCES

Batchelor, R. A., Caswell, J. L., Haynes, R. F., Wellington, K. J., Goss, W. M., & Knowles, S. H. 1980, Australian J. Phys., 33, 139
Belloni, T., & Mereghetti, S. 1994, A&A, 286, 935
Benjamin, R. A., et al. 2003, PASP, 115, 953
Blondin, J. M., & Marks, B. S. 1996, NewA, 1, 235
Brand, J., & Blitz, L. 1993, A&A, 275, 67
Carraro, G., & Munari, U. 2004, MNRAS, 347, 625
Caswell, J. L. 1997, MNRAS, 289, 203
———. 1998, MNRAS, 297, 215
Caswell, J. L., & Haynes, R. F. 1987, A&A, 171, 261
Draine, B. T. 2003, ARA&A, 41, 241
Fazio, G. G., et al. 2004, ApJS, 154, 10
Garcia-Segura, G., & Franco, J. 1996, ApJ, 469, 171
Goldwurm, A., Caraveo, P. A., & Bignami, G. F. 1987, ApJ, 322, 349
Goss, W. M., Radhakrishnan, V., Brooks, J. W., & Murray, J. D. 1972, ApJS, 24, 123
Goss, W. M., & Shaver, P. A. 1970, Australian J. Phys. Astrophys. Suppl., 14, 1
Haynes, R. F., Caswell, J. L., & Simons, L. W. J. 1978, Australian J. Phys. Astrophys. Suppl., 45, 1
———. 1979, Australian J. Phys. Astrophys. Suppl., 48, 1
Hertz, P., & Grindlay, J. E. 1984, ApJ, 278, 137
Hertz, P. L. 1983, Ph.D. thesis, Harvard Univ.
Hester, J. J., et al. 1996, AJ, 111, 2349
Manchester, R. N., Goss, W. M., & Robinson, B. J. 1969, Astrophys. Lett., 3, 11
Manchester, R. N., Robinson, B. J., & Goss, W. M. 1970, Australian J. Phys., 23, 751
McClure-Griffiths, N. M., Green, A. J., Dickey, J. M., Gaensler, B. M., Haynes, R. F., & Wieringa, M. H. 2001, ApJ, 551, 394
Mercer, E. P., et al. 2004, ApJS, 154, 328
Moffat, A. F. J., Shara, M. M., & Potter, M. 1991, AJ, 102, 642 (MSP91)
Moffat, A. F. J., & Vogt, N. 1975, A&AS, 20, 125
Reynolds, R. J. 1984, ApJ, 282, 191
Reynolds, R. J., Scherb, F., & Roesler, F. L. 1973, ApJ, 185, 869
Rodgers, A. W., Campbell, C. T., & Whiteoak, J. B. 1960, MNRAS, 121, 103
Scowen, P. A., et al. 1998, AJ, 116, 163
Shaver, P. A., & Goss, W. M. 1970, Australian J. Phys. Astrophys. Suppl., 14, 77
Stetson, P. B. 1987, PASP, 99, 191
Vacca, W. D., Garmany, C. D., & Shull, M. J. 1996, ApJ, 460, 914
van der Hucht, K. 2001, NewA Rev., 45, 135
Vishniac, E. T. 1994, ApJ, 428, 186
Westerlund, B. 1960, Ark. Astron., 2, 419
Whiteoak, J. B., & Gardner, F. F. 1974, A&A, 37, 389
Whiteoak, J. B. Z., & Uchida, K. I. 1997, A&A, 317, 563 (WU97)
Whitney, B. A., et al. 2004, ApJS, 154, 315
Wilson, T. L., Mezger, P. G., Gardner, F. F., & Milne, D. K. 1970, A&A, 6, 364

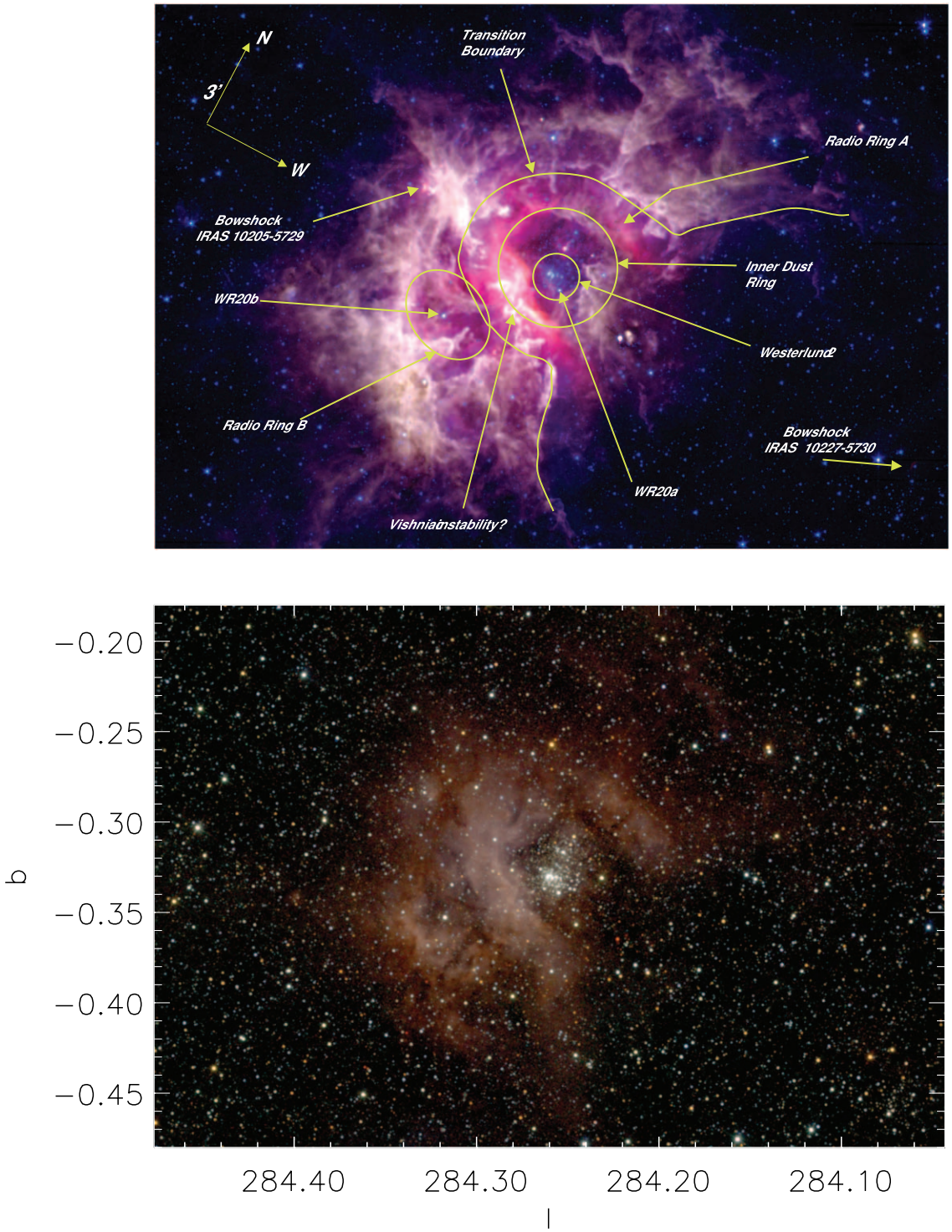

FIG. 1.—*Top*: Three-color ([3.6], [5.8], and [8.0]) image of RCW 49 with various features referred to in the text indicated by labeled arrows. Scaling is logarithmic and units are in MJy sr^{-1} for this figure and Fig. 2. *Bottom*: Three-color (*J*, *H*, and *K*) 2MASS image of RCW 49 with a similar field of view as shown in the top panel. The minimum and maximum values for all three bands are 0.5 and 700 MJy sr^{-1}.

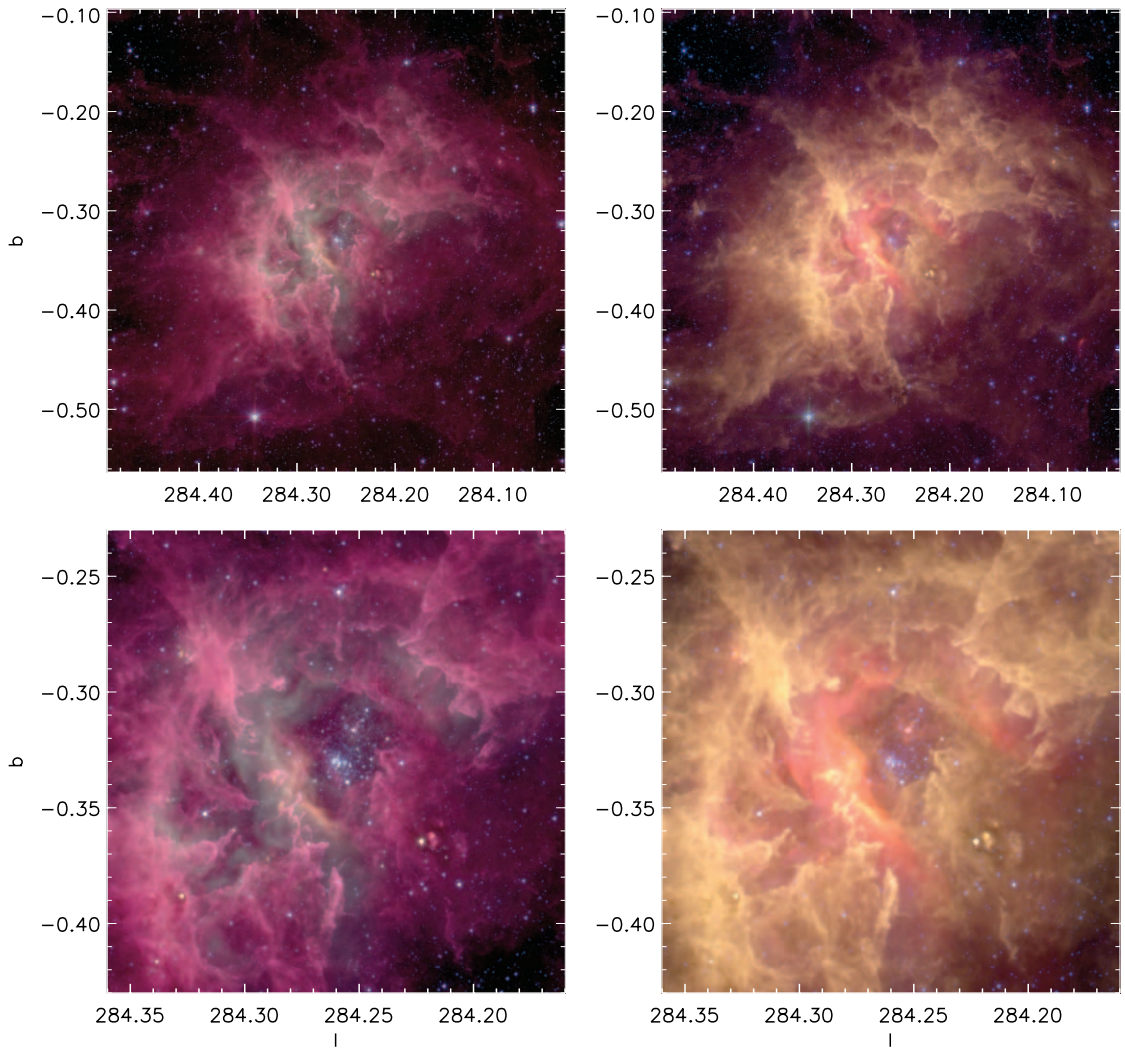

FIG. 2.—Montage of three-color images of RCW 49. *Top left*: Wide-field image showing the total extent of RCW 49 at [3.6], [4.5], and [5.8]. The minimum values displayed for each band are, respectively, 1.5, 3, and 5 MJy sr^{-1}. The maximum values are 700 for all images in this figure. *Bottom left*: Zoomed-in version of the above image centered on the W2 cluster. The minimum values for each band are 2, 6, and 10. Right panels are same as the left panels, except the IRAC bands are [3.6], [5.8], and [8.0]. *Top right*: Minimum values for each band are 1, 10, and 14. *Bottom right*: Minimum values are 1.5, 10, and 20.